Available online at www.sciencedirect.com
ScienceDirect
Lithos 96 (2007) 108–126
LITHOS
www.elsevier.com/locate/lithos

Geochemistry of Cenozoic basalts and mantle xenoliths in Northeast China

Yang Chen [a], Youxue Zhang [a,b,*], David Graham [c], Shangguo Su [d], Jinfu Deng [d]

[a] Department of Geological Sciences, The University of Michigan, Ann Arbor, MI 48109-1005, USA
[b] Key Laboratory of Orogenic Belts and Crustal Evolution, MOE, School of Earth and Space Sciences, Peking University, Beijing, 100871, China
[c] College of Oceanic and Atmospheric Sciences, Oregon State University, Corvallis, OR 97331, USA
[d] China University of Geosciences, 29 Xueyuan Road, Beijing 100083, China

Received 31 December 2005; accepted 5 September 2006
Available online 26 December 2006

Abstract

Volcanic activity in Northeast China and adjacent regions is widespread, with eruption ages ranging from Late Cretaceous (80 Ma) to about 300 years ago. Volcanic rock types are principally basanite, alkali olivine basalt, and tholeiite, with minor evolved trachyte and rhyolite. Ultramafic xenoliths, mainly spinel lherzolite and harzburgite, are common in alkali olivine basalt and basanite.

We present new major and trace element data from 11 volcanic fields, and helium isotope data from ultramafic xenoliths of three of those fields. $^{3}He/^{4}He$ ratio ranges from 5 to 7 times the atmospheric ratio, indicating that previously reported high $^{3}He/^{4}He$ ratios are likely due to the contamination by cosmogenic ^{3}He. There is currently no evidence for a high-$^{3}He/^{4}He$ mantle plume component beneath NE China. Sr–Nd–Pb isotopic data from the literature are reinterpreted to result from mixing between a FOZO end-member and a LoMu end-member. The LoMu end-member appears to reside within continental lithosphere. Major and trace elements do not indicate significant contributions from a subducted slab. Differences in depth and the extent of partial melting in the asthenosphere, both locally within individual fields and regionally between the different volcanic fields, explain most of the correlations between major and trace elements observed in this study, with deeper melting usually associated with a smaller degree of melting. Highly potassic basalts are associated with the LoMu end-member and are interpreted to be the products of lithosphere melting.

Keywords: Volcanism; Greater Northeast China; Helium isotopes; FOZO; LoMu; Low-μ; Lithosphere delamination

1. Introduction

The origin of intraplate volcanism is diverse and not always well understood. Most intraplate volcanos have been attributed to (i) mantle plumes and hot spots, such as Hawaii and Yellowstone; (ii) continental rift, such as the East Africa Rift; (iii) back-arc extension and (iv) lithosphere delamination and thinning, such as the Basin and Range. Although volcanism at intraplate settings is less common than along mid-ocean ridges and subduction zones, it is of significant importance, for both preventing geological hazards and understanding mantle geochemistry.

One notable region of intraplate volcanism is Northeast China and adjacent areas, as part of the larger volcanic belt along the eastern Asian continental margin. Recent basaltic volcanism in Northeast China surrounding NE China Plain

* Corresponding author. Department of Geological Sciences, The University of Michigan, Ann Arbor, MI 48109-1005, USA. Tel.: +1 734 763 0947; fax: +1 734 763 4690.
E-mail address: youxue@umich.edu (Y. Zhang).

0024-4937/$ - see front matter © 2006 Elsevier B.V. All rights reserved.
doi:10.1016/j.lithos.2006.09.015

was widespread although volumetrically small. In an area of about two million square kilometers, there are over 590 volcanos with volcanic rocks covering about 50,000 km^2 (Liu, 1999). The ages of tholeiitic and alkali basalts vary from about 80 Ma to about 300 years ago. (Volcanic rocks before 80 Ma are calc-alkaline, Ma et al., 2002.) For simplicity, the volcanic area will be referred to as Greater NE China (Fig. 1); volcanic rocks south of this region (e.g., Zou et al., 2000) will not be included. The activity of each volcanic field varies significantly. Some large volcanic fields were active for tens of million years, while some small ones lasted for less than 1 Myr. The major types of the volcanic rocks are basanite, alkali olivine basalt, and tholeiite, with minor evolved trachyte and alkaline to peralkaline rhyolite. Ultramafic xenoliths, mainly spinel lherzolite and harzburgite, are common in basanite and alkali olivine basalt (e.g., Fan and Hooper, 1989).

Greater NE China lies on two tectonic units: (i) North China–Korea Craton (NCKC) and (ii) Central Asian Orogenic Belt (CAOB, Sengor and Natal'in, 1996). NCKC formed during the Archean and early Proterozoic. CAOB is interpreted to be an intercontinental fold belt that underwent collision and subduction among Siberian Craton, NCKC and other smaller Mongol–Okhotsk blocks. NCKC and CAOB became part of Eurasia plate as the Mongolo–Okhotsk Ocean closed during early-Cretaceous (e.g., Yin and Harrison, 1996). In late Mesozoic to Cenozoic, tectonic evolution of East Asia is controlled by (i) indentation of the Indian plate and (ii) subduction of the Pacific plate and Philippine Sea plate. At about 80 Ma (but not necessarily at the same time for different regions), volcanic rocks in NE China changed composition from dominantly calcalkaline series to dominantly alkali series. These more recent volcanic rocks are the focus of this work.

In addition to field studies and geochronology, numerous geochemical investigations on the volcanic rocks have been carried out. Based on major and trace elements, the rocks are highly enriched in incompatible elements

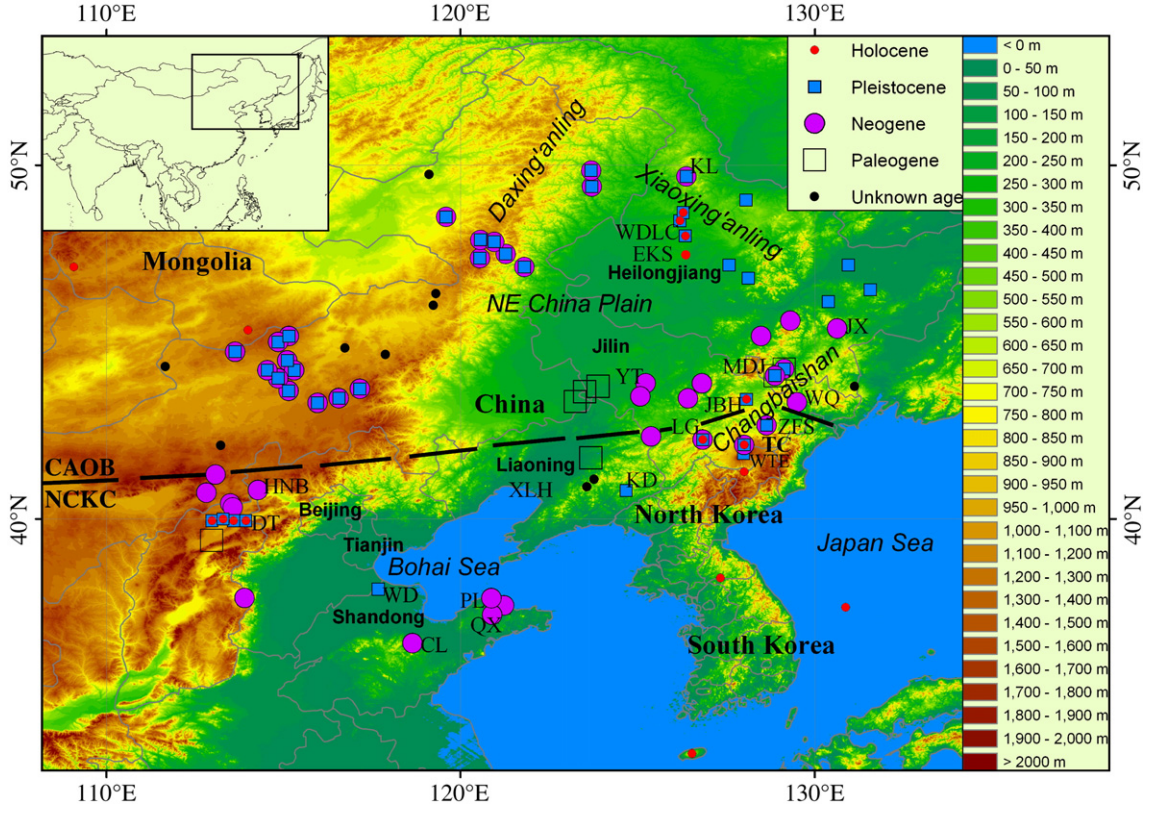

Fig. 1. A topography map of Greater Northeast China with volcanic fields indicated. Dashed line is the approximate boundary between North China–Korea Craton and Central Asian Orogenic Belt. Abrreviations of volcanic fields are as follows: KL (Keluo), **WDLC (Wudalianchi)**, **EKS (Erkeshan)**, **JX (Jixi)**, **MDJ (Mudanjiang)**, WQ (Wangqing), YT (Yitong), **JBH (Jingbohu)**, **CBS** (**Changbaishan**, including TC (Tianchi), ZFS (Zengfengshan) and WTE (Wangtian'e)), **LG (Longgang), KD (Kuandian)**, XLH (Xialiaohe, borehole samples), **CL (Changle), WD (Wudi)**, PL (Penglai), QX (Qixia), HNB (Hannuoba), and **DT (Datong)**. Bold-face type indicates that the volcanic field has been sampled in this work. Sources of age data can be found in Appendix 2 (online).

(e.g., Zhou and Armstrong, 1982; Basu et al., 1991; Liu, 1992; Jin and Zhang, 1994; Liu, 1995, 1999). Based on Sr–Nd–Pb isotopic data (e.g., Zhou and Armstrong, 1982; Peng et al., 1986; Basu et al., 1991; Zhang et al., 1991; Tu et al., 1992), significant contamination by continental crust was ruled out, and it was suggested that the mantle may be viewed as a two end-member mixture between a depleted mantle and an enriched mantle EM1 (Basu et al., 1991). Helium isotope data (Xu et al., 1998a; Li et al., 2002; Xu and Liu, 2002; Wu et al., 2003; Lai et al., 2005) are scattered, and some seem to indicate a possible high-$^3He/^4He$ plume component. The most extreme helium data are those of Li et al. (2002), with the $^3He/^4He$ ratio varying widely from 0.1 to 700 times the atmospheric ratio.

The origin of intraplate volcanism in this region is under debate. There are numerous hypotheses to explain the diffuse volcanism in Greater NE China, including but not limited to, mantle plume or hotspot (e.g. Deng et al., 1996, 2004), back-arc extension caused by subduction of Kula–Pacific plate (e.g., Liu, 1987; Liu et al., 2001; Ren et al., 2002), mantle upwelling while crossing from a thick lithosphere to a thin lithosphere (Niu, 2005), and thinning/delamination of the lithosphere beneath Northeast mainland Asia from a thickness of about 200 km in Paleozoic to about 80 km in the present (e.g., Menzies et al., 1993; Griffin et al., 1998; Menzies and Xu, 1998; Wilde et al., 2003). In this work we report new major and trace element data, and helium isotopic data. We discuss literature data quality, investigate the mantle characteristics using our data and literature data, and examine the origin of volcanism in Greater NE China.

2. Samples and analytical methods

2.1. Samples

Our own samples come from eleven volcanic fields. They are, from North to South, Wudalianchi (WDLC), Erkeshan (EKS), Mudanjiang (MDJ), Jixi (JX), Jingbohu (JBH), Changbaishan (CBS), Longgang (LG), Kuandian (KD), Datong (DT), Wudi (WD), and Changle (CL) (Fig. 1). Because of compositional similarities, WDLC and EKS are often combined, so are MDJ and JX, and WD and CL. No attempt was made to map and sample every volcanic field systematically. The samples are mainly Quaternary in age, except for those from MDJ, JX, and CL, and some from CBS. A brief description of each of the sampled volcanic fields can be found in Appendix 1 (online).

Basalt samples were collected from fresh outcrops including quarries and road cuts. Most basaltic samples are aphyric with microphenocrysts (≤ 0.2 mm) of olivine, plagioclase and clinopyroxene. Fe–Ti oxides exist in some samples. Mantle xenolith samples for $^3He/^4He$ isotope analyses are collected from quarries, fresh road cuts and deep gullies. No other isotopic data were obtained, but literature data will be used in exploring mantle characteristics.

2.2. Major and trace element analyses

Fresh basalt samples were cut and cleaned for major and trace elements analysis. Major elements plus Rb, Sr and Zr were analyzed by X-ray fluorescence method (XRF). Other trace elements were analyzed by Inductively Coupled Plasma Mass Spectrometry (ICP-MS). Most samples were analyzed at Michigan State University following the procedures of Hannah et al. (2002). In order to check the accuracy of the analyses, selected samples were re-analyzed at Washington State University—Pullman following the procedures of Knaack et al. (1994). The results are shown in Table A1 (online). Standards BCR-2, BHVO-2, K1919, NKT-1 are measured as unknowns and are compared with reference values from USGS and literature in Table A1a.

The quality of the analyses is assessed by a number of ways: (1) by comparisons between standards analyzed as unknowns and published reference values (Table A1a); (2) by comparison between MSU and WSU analyses of the same rocks; and (3) by repeated analyses of the same rock. Furthermore, if trace element relations appeared peculiar, attempts were made to check the data. For example, some data from the MSU lab showed a significant positive Yb anomaly. We sent some of the same samples to WSU and found that such anomalies are not present. Based on these assessments, the accuracy is within 3% relative for SiO_2, TiO_2, Al_2O_3, MgO, and CaO; 5% for P, Mn, Y, Cu, and Zn; 10% for Fe_2O_3, K, Sr, Nb, La, and Ce; 15% for Nd, Zr, Ba, Th, Ta, Pr, Sm, Ho, Er, and Hf; 20% for Eu, Na, Tb, Dy, V, Sc, and Ga; and 25% for Ho and Gd. The uncertainty for Tm is not known, but repeated analyses agree well. Concentrations of other elements (Ni, Cr, Rb, Yb, Lu, Pb, and U) are more uncertain and are not reported in Table A1b.

2.3. Helium isotope analyses

In order to test whether a high-$^3He/^4He$ mantle plume component is present, we collected mantle xenoliths and carried out He isotopic analyses on 8 mantle xenoliths from JBH (2 samples), KD (3 samples) and LG (3 samples) volcanic fields. Large and relatively fresh olivine crystals, typically about 1 mm in maximum size, were hand-picked from crushed xenolith samples under

Table 1
Helium isotope data in mantle xenoliths from NE China

Location and Sample name	Latitude (°N)	Longitude (°E)	Weight (mg)	^{4}He 10^{-9} cc/g	^{3}He 10^{-14} cc/g	^{3}He/^{4}He (Ra)±2σ
KD-HY-2a-2	40.72339	124.76103	470.6	9.53	9.27	7.00±0.17
KD-HY-2b-1	40.72339	124.76103	500.9	2.30	1.81	5.67±0.40
KD-HY-4d	40.72194	124.76117	485.3	0.433	0.289	4.80±1.55
LG-DLW-1d-1	42.33611	126.41672	452.1	4.13	3.16	5.50±0.29
LG-DLW-1f	42.33611	126.41672	477.4	6.98	5.58	5.75±0.18
LG-DLW-1q	42.33611	126.41672	393.6	3.26	2.72	6.01±0.38
JBH-3i-1	44.19588	128.52737	460.0	1.95	1.68	6.21±0.52
JBH-3i-5	44.19588	128.52737	393.6	0.289	0.290	7.23±2.60

All analyses were performed on hand-picked olivine grains from lherzolite (KD and JBH) or harzburgite (LG) by in vacuo crushing using ~200 high impact strokes. Uncertainties are the quadrature sum of in run statistics plus uncertainties associated with air standards and blanks. The sample name can be decoded as follows: KD-HY-2 means fieldwork stop 2, Huangyishan (HY) in the Kuandian (KD) volcanic field, and LG-DLW-1 means fieldwork stop 1, Dalongwan (DLW) in the Longgang (LG) volcanic field.

a binocular microscope. The range of sample sizes analyzed was between 0.4 and 0.5 g. To avoid possible contamination from adhering groundmass of the host basalt or from dust, olivine grains were first ultrasonically cleaned in 1 M HCl for 15 to 30 min, and then rinsed successively by deionized water and ethanol. The final products were re-examined under the microscope to ensure the absence of foreign material.

The helium isotope analyses were performed at NOAA/PMEL in Newport, Oregon following procedures described previously (Graham et al., 1998). All gas extractions were performed by crushing in vacuum to liberate helium trapped in melt and fluid inclusions. After loading the sample into a stainless steel chamber together with a magnetic piston, the piston was lifted and dropped about 200 times under vacuum using a system of external solenoids, crushing the sample to a powder. Non-condensable, reactive gases were gettered over hot Ti; Ar, Kr and Xe were trapped on activated charcoal using liquid N_2; and neon was separated onto a cryogenically-controlled charcoal trap at 38 K. The helium was admitted directly to the mass spectrometer for isotope ratio and peak height (concentration) determination. The vacuum line blank for crushing was $<1\times10^{-10}$ ccSTP for ^{4}He, and line blanks were run before and after all samples. Simultaneous measurement of ^{3}He and ^{4}He was performed on a double collector mass spectrometer especially designed for high precision helium isotope analysis by J. E. Lupton. The instrument is equipped with a Baur–Signer ion source (manufactured by ETH, Zurich) that contributes to its high sensitivity, high linearity, and low mass discrimination. The collector section is fitted with a Johnston electron multiplier attached to ion counting electronics and a Faraday cup. The sensitivity for helium is $>10^{-4}$ A/Torr, while the absolute detection limit is $<5\times10^4$ atoms ^{3}He. The He isotope data are reported in Table 1.

In summary, care was taken during both sample collection and analyses to avoid cosmogenic ^{3}He. (1) Because cosmic ray spallation may produce ^{3}He in old exposed surface rocks (to about 1 m depth), samples were collected in quarries, fresh road cuts and deep gullies (presumably rapidly eroded), and hence may be assumed to contain negligible amounts of cosmogenic ^{3}He. (2) For helium isotope analyses, the crushing technique that releases ^{3}He in fluid inclusions is used, instead of the melting technique that releases ^{3}He in both inclusions and the lattice. Because cosmogenic ^{3}He is dominantly located within the crystal lattice, the crushing method minimizes the contribution from cosmognic ^{3}He.

3. Results

3.1. Major oxides

Major oxide concentrations from this work are shown in Fig. 2 in a diagram of total alkalis versus

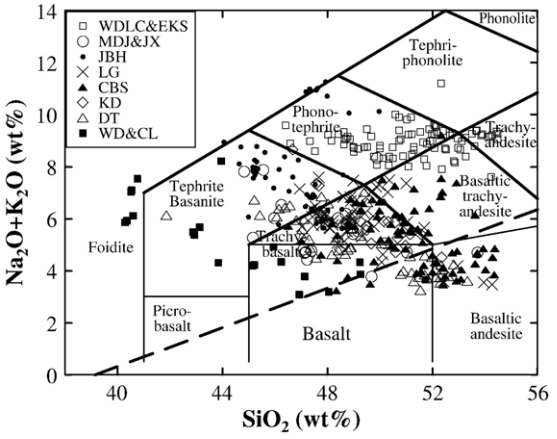

Fig. 2. Total alkalis versus SiO_2. Lines and fields are based on Le Bas et al. (1986). Data sources can be found in Appendix 2 (online).

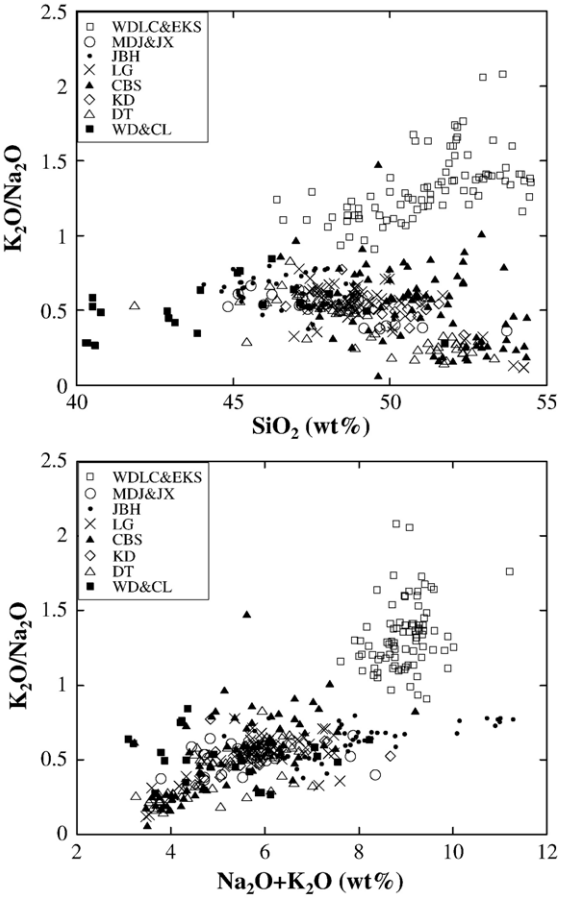

Fig. 3. K_2O/Na_2O ratio versus SiO_2 and total alkalis for Greater NE China volcanic rocks with $SiO_2 < 55\%$. See Fig. 1 for abbreviations of the volcanic fields. Data sources can be found in Appendix 2 (online).

SiO_2. Also shown are literature data we have compiled. As recognized by previous authors and shown in Fig. 2, the volcanic rocks in NE China are diverse, ranging from tholeiitic to alkaline to peralkaline. Specifically, Wudalianchi and Erkeshan basalts are highly potassic (Fig. 3), Wudi rocks are low in SiO_2, and the rest are more "normal" alkali and tholeiitic basalts.

Fig. 4 shows major oxides plotted against MgO concentration. SiO_2 is negatively and CaO is positively correlated with MgO. The upper limit of K_2O decreases linearly with MgO. For each volcanic field, Al_2O_3 is linearly anticorrelated with MgO (Fig. 4). At a given MgO, Al_2O_3 concentration is lowest at WDLC and EKS, and highest at LG. The difference in Al_2O_3 at the same MgO probably reflects difference in melting conditions. At a given MgO, WDLC-EKS and WD display the highest K_2O, and DT and CBS show the lowest K_2O. WD samples also exhibit high Na_2O and P_2O_5 for its very high MgO concentration.

3.2. Trace elements

Trace element concentrations are reported in Table A1b (online). Selected trace elements and major elements are plotted in Fig. 5. Some trace elements are well correlated. Hf and Zr are well correlated with Hf/Zr ratio slightly below chondrite ratio (Fig. 5C). Fig. 5D shows that Ta and Nb are well correlated with Nb/Ta ratio of 17.3 (scatter of ±25%), in agreement with the chondritic ratio of 17.8 (McDonough and Sun, 1995).

In K_2O versus SiO_2 (Fig. 5A), WD, CL, JBH, WDLC and EKS form a positive correlation trend, whereas MD, JX, DT, CBS, and KD show a negative correlation trend. Every volcanic filed seems to trend toward a focal zone of (46±2)% SiO_2 and (2.8±0.5)% K_2O. Nb and some other incompatible trace elements (Ta, La, Ce, Th) are in general negatively correlated with SiO_2 (Fig. 5B). The negative correlation will be addressed in the Discussion.

Most trace element data are shown in Fig. 6 as "spidergrams" by normalizing to concentrations in the bulk silicate Earth (BSE) (McDonough and Sun, 1995). Elements with compatibility in between REE (such as Zr, Hf, P, Ti, and Y) are not plotted so that the REE part is clearly shown in Fig. 6, eliminating the need for a separate REE plot. Lu concentration data have large uncertainties (as high as 40% relative) and are not reported in Table A1. Nevertheless, Lu is still shown in the spidergrams to complete the REE pattern. (Yb is not shown because the measurement uncertainty is even larger.) Not all the patterns are identical in shape. One general feature is the strong enrichment in LREE and other incompatible elements in recent basalts from Greater NE China. There is more enrichment in LREE in WDLC, EKS, and JBH, than in DT. When the LREE enrichment is less strong, the absolute concentration of HREE is slightly higher, leading to cross patterns (Fig. 6G), suggesting that partial melting occurred at different depths with different partition coefficients. There is no depletion in high field strength elements (HFSE) such as Nb and Ta except for WDLC and EKS regions. There is no excess enrichment of large ion lithophile elements (LILE) such as Ba and K, except for both enrichment and depletion of K in CBS, and depletion of K in CL and WD. In some volcanic fields, there are depletions of Ba and Th compared to the extrapolated REE patterns. The difference between the volcanic fields will be discussed later.

3.3. Helium isotopic data

$^3He/^4He$ ratios in xenoliths from three of the volcanic fields (Kuandian, Longgang, and Jingbohu) are

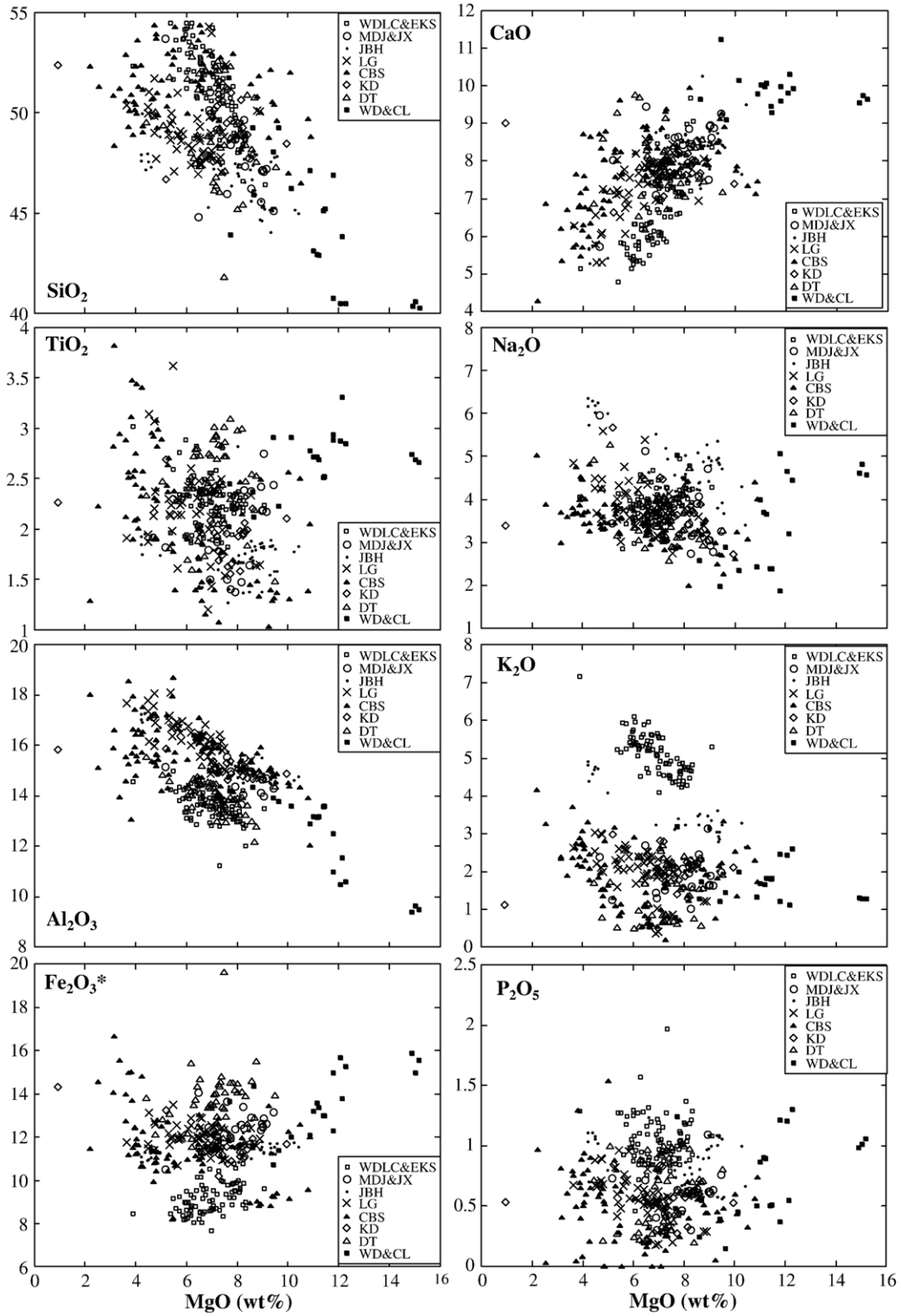

Fig. 4. SiO_2, TiO_2, Al_2O_3, Fe_2O_3*, CaO, Na_2O, K_2O, and P_2O_5 versus MgO. See Fig. 1 for abbreviations of the volcanic fields. Data sources can be found in Appendix 2 (online).

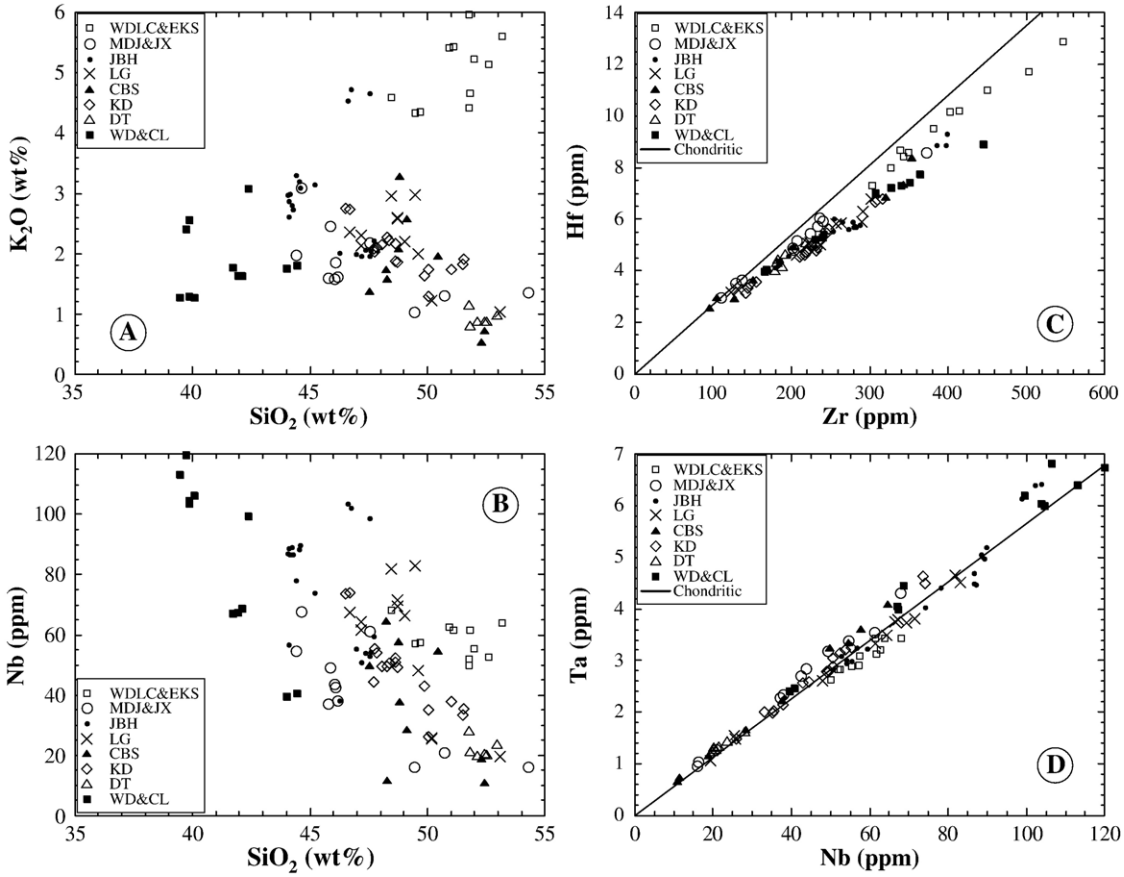

Fig. 5. Selected elemental plots. See Fig. 1 for abbreviations of the volcanic fields. Data are from this work.

relatively uniform, ranging from 4.8±1.6 R_A to 7.0±0.2 R_A times the atmospheric ratio (R_A) at KD (reported analytical uncertainties are 2σ), from 5.5±0.3 to 6.0±0.4 at LG, and from 6.2±0.5 to 7.2±2.6 at JBH. There is no systematic correlation with helium abundance, although the two analyses with the largest uncertainties are for samples with [He] below 5×10^{-10} ccSTP/g. Based on these data there does not appear to be a difference in $^3He/^4He$ between the 3 localities. Most significantly, no high $^3He/^4He$ ratios have been measured in this study, in which samples were collected from freshly exposed surfaces and all gas extractions were performed by crushing to minimize the signal of cosmogenic ^3He.

4. Discussion

4.1. Helium isotope characteristics

Helium isotopic ratios are a useful tracer of mantle source regions. In addition to primordial ^3He and ^4He, ^4He is produced by radioactive decay of U and Th. Hence in the Earth's interior the $^3He/^4He$ ratio decreases with time due to radioactive decay. A larger (U+Th)/^3He ratio leads to a more rapid decrease of $^3He/^4He$ ratio. The $^3He/^4He$ ratio in the mantle, as sampled by basalts, mantle xenoliths and volcanic gases, is greater than that in the atmosphere or the crust, due to primordial ^3He still trapped in the mantle and rapid ^3He escape from the atmosphere (Clarke et al., 1969). The $^3He/^4He$ ratio in mid-ocean ridge basalts away from the influence of ocean island hotspots is relatively uniform, between 6 to 10 times the atmospheric ratio (Graham, 2002). The highest $^3He/^4He$ in the source regions of island arcs is typically at the low end of the MORB range (Poreda and Craig, 1989; Porcelli et al., 1992), and ranges to considerably lower ratios (Hilton and Craig, 1989) due to the presence of radiogenic helium derived either from shallow levels in the crust or from subducted material. In contrast, mantle plumes sampled at ocean islands such as Hawaii and Iceland display $^3He/^4He$ ratios higher than those in MORB

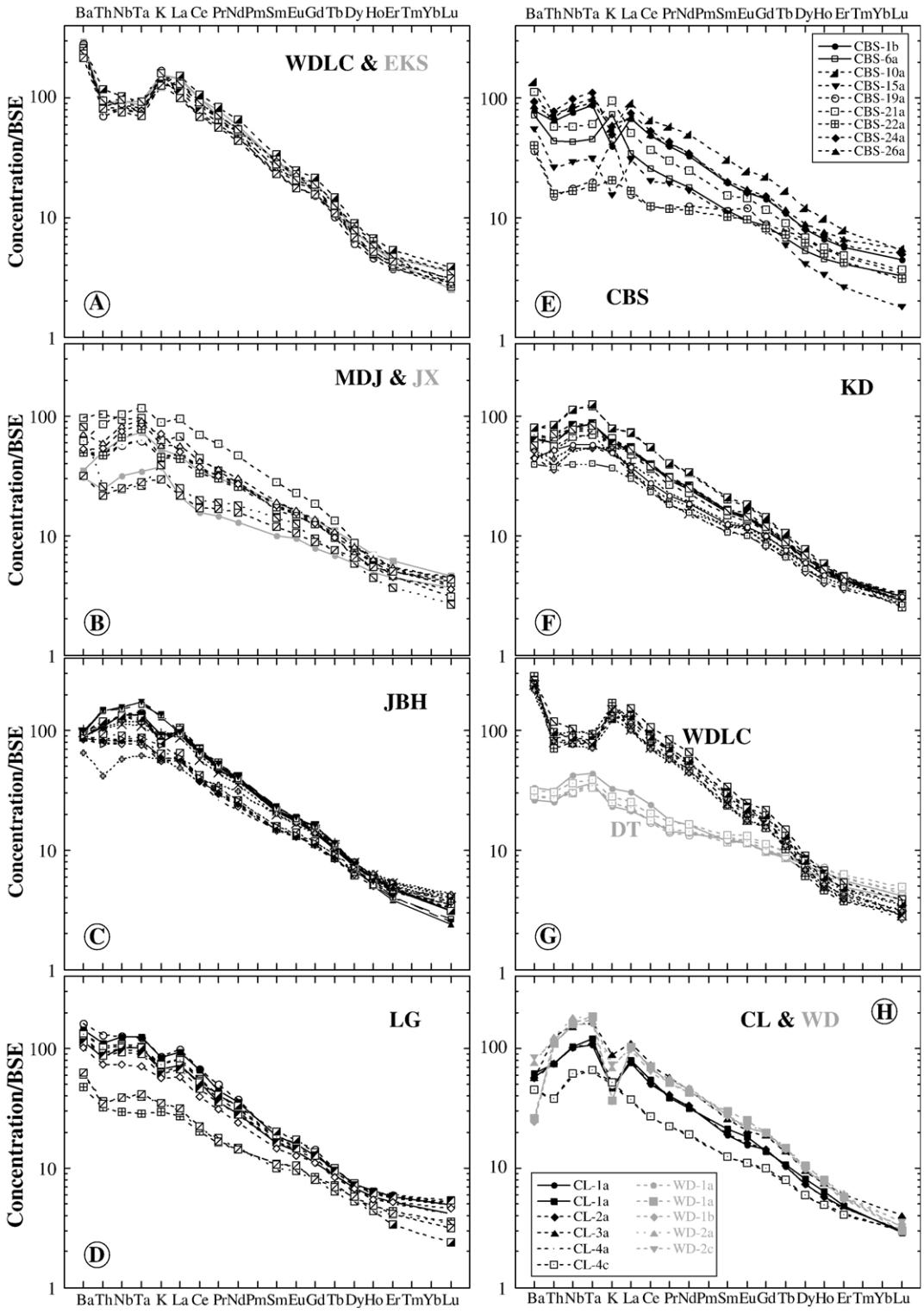

Fig. 6. Spidergram normalized to the concentration of bulk silicate Earth (McDonough and Sun, 1995). See Fig. 1 for abbreviations of the volcanic fields. Data are from this work.

(Kurz et al., 1983; Hilton et al., 1999). Such high ratios are usually considered to reflect a relative ^{3}He enrichment in less degassed and presumably deeper mantle sources of the plumes (e.g., Kurz et al., 1982; Class and Goldstein, 2005).

A possible complication of ^{3}He/^{4}He isotopic analyses of subaerial rocks is the presence of cosmogenic ^{3}He, produced primarily via spallation reactions on O, Mg and Si in silicates due to the penetration of secondary neutrons that were ultimately produced by cosmic rays in the atmosphere. The characteristic (e-folding) penetration distance is about 0.5 m, and results in a ^{3}He production rate of 100 atoms·g^{-1}·yr^{-1} in silicates exposed at the Earth's surface (Kurz, 1986). While cosmogenic ^{3}He is useful in determining exposure ages, it needs to be avoided in understanding mantle ^{3}He/^{4}He characteristics from rocks exposed at the Earth's surface.

Previous ^{3}He/^{4}He results for mantle xenoliths from Greater Northeast China basalt are complicated by the possible presence of cosmogenic ^{3}He. Porcelli et al. (1987) reported a ^{3}He/^{4}He ratio in a spinel lherzolite from Northeast China of (49±16) R_A. They assumed that the initial ratio before exposure to cosmic ray bombardment to be 8 R_A, and found that the excess ^{3}He was consistent with derivation from in situ cosmic ray spallation. Shangguan et al. (1998) reported ^{3}He/^{4}He ratios in Changbaishan hot springs to be (5.6±0.3) R_A, consistent with the xenolith results reported here. Xu et al. (1998a) analyzed ^{3}He/^{4}He by melting of samples, and found ratios ranging from 8.9 to 11.3 R_A for pyroxenite and lherzolite xenoliths from Kuandian basalts, and 4.3 to 6.6 R_A for xenoliths from Longgang (also called Huinan) basalts. Li et al. (2002) also analyzed samples by the melting technique, and reported ^{3}He/^{4}He between 7.5 and 24 (±26) R_A for megacrysts from Kuandian, and 0.11 to 5.3 R_A for xenoliths, and 4.1 to 694 (±13) R_A for megacrysts from Hannuoba. Xu et al. (1998a) discussed the issue of cosmogenic ^{3}He inconclusively, and mentioned that analyses of the samples by crushing would resolve the issue. Li et al. (2002) did not address the presence of cosmogenic ^{3}He at all. The ^{3}He/^{4}He results for Longgang by Xu et al. (1998a) are in agreement with our results, but those for Kuandian by Xu et al. (1998a), Li et al. (2002) differ from ours (Fig. 7) and may be explained by the presence of small amounts of cosmogenic ^{3}He in those earlier analyses. Wu et al. (2003) measured ^{3}He/^{4}He ratios in augite megacrysts, peridotite and alkali basalts in Kuandian using the melting technique, and obtained ratios of 10 R_A for augite megacryst, 2.6 to 4.5 R_A for peridotite, and 0.5 to 0.6 R_A for alkali basalts. Lai et al. (2005) determined ^{3}He/^{4}He ratios in olivine, orthopyroxene and clinopyroxene of mantle xenoliths from both Kuandian and Wudalianchi using the crushing technique, and found the ratio to be between 4.5 and 7.5 R_A, similar to our data for Kuandian, Longgang and Jingbohu. Because we have taken care to avoid cosmogenic ^{3}He in both sample collection and analyses, we interpret our crushing results to reflect mantle characteristics, whereas the higher ^{3}He/^{4}He ratios (>8 R_A) in some previous papers likely reflect some unknown amount of contamination by cosmogenic ^{3}He, and the lower ratios reflect crustal contamination.

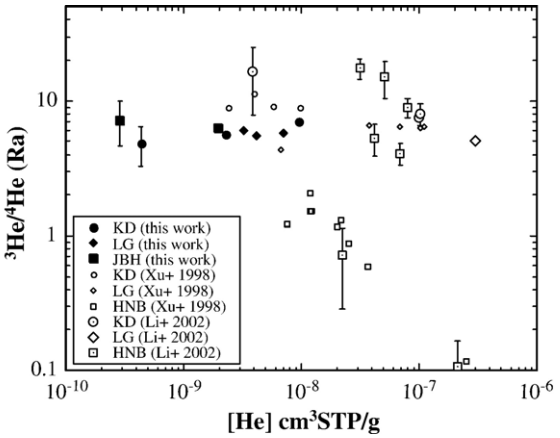

Fig. 7. Helium isotopic data. Solid symbols are data from this work with ^{3}He/^{4}He analyzed by crushing. Open symbols are literature data from Xu et al. (1998a), Li et al. (2002) with ^{3}He/^{4}He analyzed by melting. Two data points from Li et al. (2002) with ^{3}He/^{4}He ratio of about 700 times Ra are not shown so that the vertical axis is not too compressed. Error bars are shown at 2σ when the error is larger than the size of the symbol. One data point with huge error is excluded.

In summary, ^{3}He/^{4}He ratios in the mantle xenoliths of the 3 volcanic fields we have studied in Northeast China range from 5.5 to 7.0 R_A. This range is significantly below the high ^{3}He/^{4}He ratios of mantle plumes such as those beneath Hawaii and Iceland. It overlaps the range for the MORB mantle, and is also similar to values in some island arc and ocean island regions. The small variation in the ^{3}He/^{4}He ratio could be attributed to in-growth of ^{4}He. There is presently no clear evidence for a high-^{3}He/^{4}He mantle plume component contributing to the volcanism in NE China, although the data coverage is still limited. Earlier claims for the presence of high ^{3}He/^{4}He ratios beneath part of Japan (proximal to NE China) were recently revisited by Yokochi et al. (2005), who also concluded that those high ratios are most likely cosmogenically derived.

Note that we, as well as previous authors, measured He isotopes in mantle xenoliths rather than in basalt

directly. Subaerial basalt groundmass does not retain its original helium (e.g., Lai et al., 2005). The mantle xenoliths were entrained as deep-sourced magma erupted and do not strictly record the intrinsic $^{3}He/^{4}He$ of the basalt mantle source. However, fluid inclusions in olivine typically undergo significant reequilibration with the host magma during ascent. We therefore assume in this reconnaissance study that the helium released by crushing of the xenoliths is representative of the helium in the mantle source region of the basalts.

4.2. Sr–Nd–Pb isotopes

We did not obtain new Sr–Nd–Pb isotopic data in this study because there is already a significant body of isotopic data for Cenozoic NE China basalts (e.g., Zhou and Armstrong, 1982; Peng et al., 1986; Liu et al., 1989; Basu et al., 1991; Zhang et al., 1991; Tu et al., 1992) and there are no special concerns about the quality of the data. In this section we examine available literature isotopic data about isotopic characteristics. Zhou and Armstrong (1982) carried out the first Sr–Nd isotopic study on recent basalts from North and Northeast China, and recognized mantle heterogeneity in eastern China. Peng et al. (1986) identified a distinct mantle component with time-integrated low U/Pb ratio. Liu et al. (1989) first proposed the presence of a LoMu component in NE China mantle. Basu et al. (1991), Zhang et al. (1991) suggested that recent basalts in eastern China can be attributed to mixing between a MORB-like reservoir (DM; depleted mantle) and an EM1 reservoir (and with significant Dupal signature). Later authors (e.g., Tu et al., 1992; Choi et al., 2005) mostly followed the interpretation of Basu et al. (1991), Zhang et al. (1991).

Fig. 8 compares literature isotopic data in recent NE China basalts with various mantle end-members. Examining Sr–Nd isotopes alone (Fig. 8A), NE China basalts (blue squares) may be viewed to be a mixture of DM and EM1, but may also be due to mixing of FOZO and LoMu. Coupling Sr–Nd and Pb isotopes (Fig. 8B, C, and D), it can be seen that NE China basalts cannot be

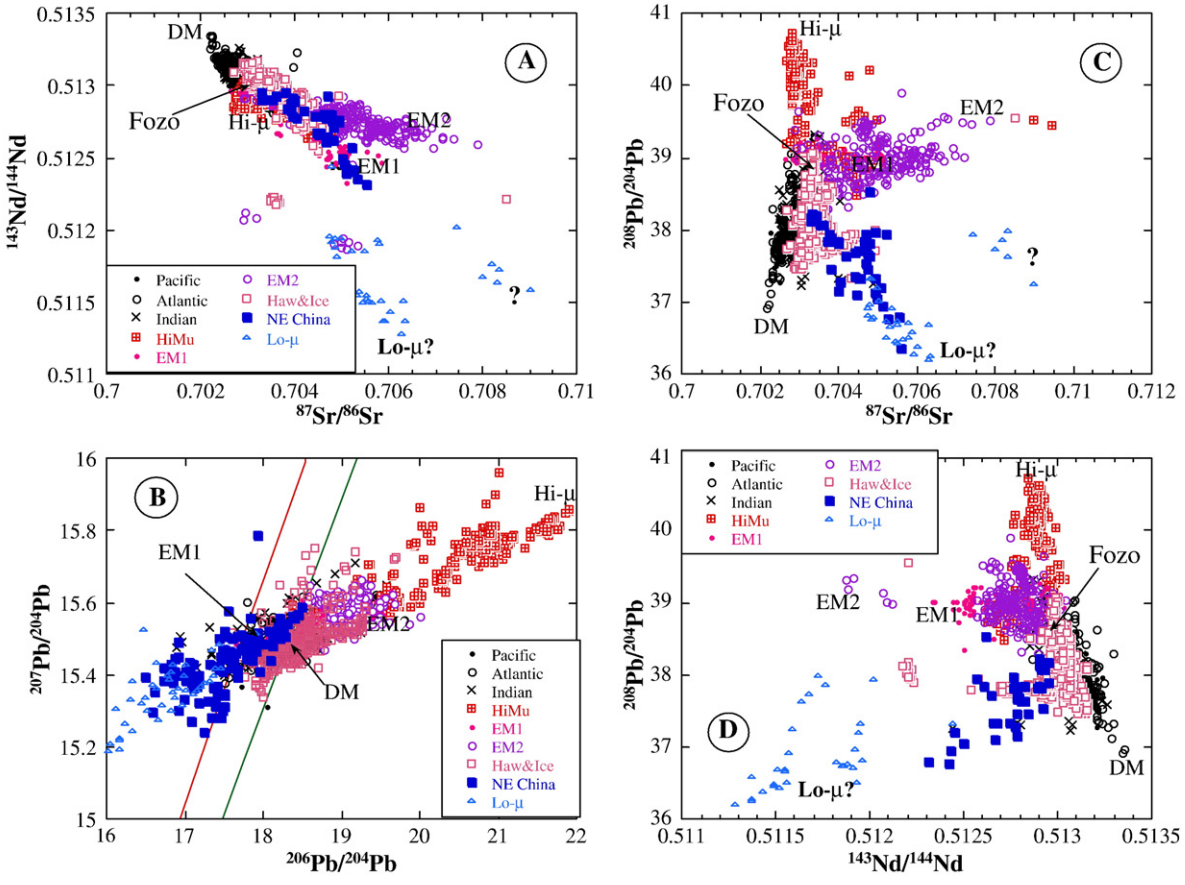

Fig. 8. Sr–Nd–Pb isotopic data. The two lines in (B) are 4.55 Ga and 4.45 Ga geochrons. Data sources can be found in Appendix 2 (online).

Table 2
Isotopic end-members

	$^{206}Pb/^{204}Pb$	$^{207}Pb/^{204}Pb$	$^{208}Pb/^{204}Pb$	$^{87}Sr/^{86}Sr$	$^{143}Nd/^{144}Nd$
LoMu, ref. 1	16.5	15.7	38.5	0.710	0.51125
LoMu, this work	16.0	15.2	36.1	0.706	0.5122
EM1, ref. 2	17.6	15.48	39	0.7055	0.5124
EM2, ref. 2	19.2	15.6	39.6	0.708	0.5126
HiMu, ref. 2	22	16	40.8	0.7028	0.5128
FOZO, ref. 3	19	15.6	39	0.7035	0.5129
DMM, ref. 2	17.5	15.38	36.9	0.7022	0.5134

References: 1. Douglass and Schilling (2000); 2. See references for Fig. 8; 3. Hauri et al. (1994), Stracke et al. (2005).

produced by mixing DM and EM1. First, the end-member with low Pb isotopic ratios in NE China differs from the EM1 end-member in $^{208}Pb/^{204}Pb$: in EM1, $^{208}Pb/^{204}Pb$ is about 38.2; but in NE China, $^{208}Pb/^{204}Pb$ is as low as 36.2, indicating a LoMu component (e.g., Doe et al., 1982; Liu et al., 1989; Zhou and Zhu, 1992; O'Brien et al., 1995; Mahoney et al., 1996; Douglass and Schilling, 2000). In literature, the end-member of low Pb isotopic ratios is often confused with the EM1 end-member. For example, Douglass and Schilling (2000) explicitly defined a LoMu end-member as $^{206}Pb/^{204}Pb=16.50$, $^{207}Pb/^{204}Pb=15.70$, and $^{208}Pb/^{204}Pb=38.5$. However, this definition is similar to EM1 with fairly high $^{207}Pb/^{204}Pb$ and $^{208}Pb/^{204}Pb$ ratios, significantly higher than the LoMu end-member in NE China and in Smoky Butte, Western US (Fig. 8). In Fig. 8, there is an end-member with low $^{206}Pb/^{204}Pb$ (16.00), low $^{207}Pb/^{204}Pb$ (15.20), and low $^{208}Pb/^{204}Pb$ (36.1), as exemplified by Smoky Buttes and pointed to by NE China basalts. This end-member, with $^{87}Sr/^{86}Sr=0.706$ and $^{143}Nd/^{144}Nd=0.5113$, is hereafter defined as the LoMu end-member (Table 2). We suggest that one isotopic end-member for NE China basalts is this LoMu, instead of EM1.

Secondly, the other end-member, with higher Pb isotopic ratios (e.g., $^{208}Pb/^{204}Pb=38.5$), lower $^{87}Sr/^{86}Sr$ and higher $^{143}Nd/^{144}Nd$, does not point to the DM end-member whose $^{208}Pb/^{204}Pb$ is only about 37. Fig. 8C shows both MORB isotopic trend and NE China trend point to and roughly meet at FOZO (Hart, 1992; Stracke et al., 2005). The concept of FOZO (Focal zone) was introduced by Hart (1992), and post-dated the work of Basu et al. (1991). Furthermore, trace elements in NE China basalts exhibit a strongly enriched signature, opposite to strongly depleted signature of MORB. In summary, (i) DM could be one end-member for the Nd–Sr isotope data, but it is not the only choice; (ii) DM cannot explain the Pb isotopic data, especially $^{208}Pb/^{206}Pb$ ratios; and (iii) trace element data do not need contribution from DM. Hence, we suggest that the other isotopic end-member in NE China basalts is FOZO. That one end-member of Greater NE China basalts is FOZO is consistent with the notion that the FOZO end-member is the focal zone from which most mantle mixing arrays emanate (Hart, 1992).

The LoMu isotopic feature is encountered in potassic basalts in continental setting. Commonly invoked LoMu source is sub-continental lithosphere (e.g., Douglass and Schilling, 2000) with the presence of a potassic phase such as phlogopite and/or amphibole (Hawkesworth et al., 1990), which may produce Ta depletion during partial melting (Class and Goldstein, 1997). These are consistent with data for WDLC and EKS (potassic rocks with Ta depletion).

Another interesting observation is that in $^{207}Pb/^{204}Pb$–$^{206}Pb/^{204}Pb$ diagram, data from NE China basalts are on both sides of the 4.55-Ga geochron, whereas literature data on MORB and OIB are mostly on the right hand side of the geochron because of the absence of the LoMu end-member in oceanic basalts. If there is enough LoMu material, then average $^{207}Pb/^{204}Pb$ and $^{206}Pb/^{204}Pb$ ratios of the bulk silicate Earth might lie on the 4.55-Ga geochron.

4.3. Major and trace elements

4.3.1. Trace element data quality

There were numerous publications of trace element data on Greater NE China basalts (see references on Fig. 9). However, the quality of literature data is not always easy to assess. Goldstein et al. (2003) published an editorial and suggested the standards for publication of chemical data. Previous workers might not have followed them. Because reanalyzing the same samples reported in literature is not a practical option, below we make rough assessment using concentration plots of two elements known to have similar compatibility. In such plots, excellent correlations are expected if data quality is high. Fig. 9A shows Ta versus Nb (literature data and our own data). The concentrations of these two elements

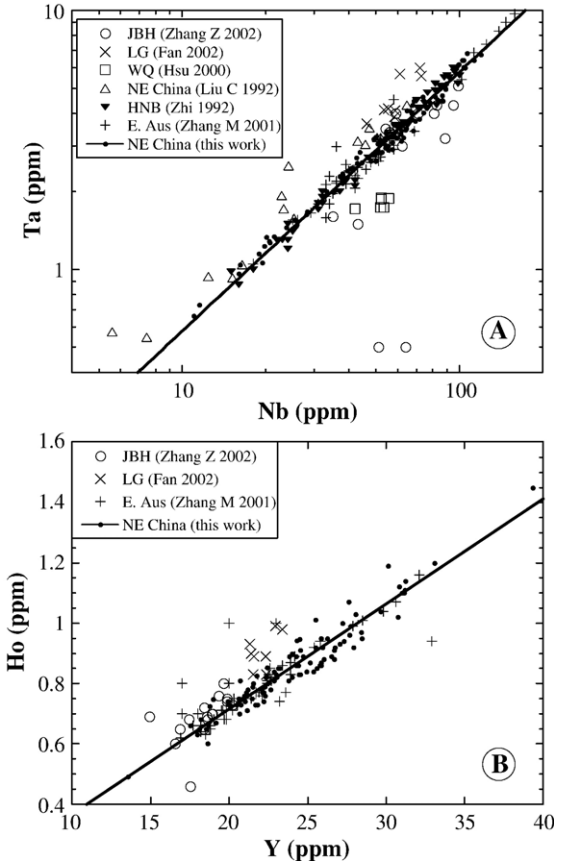

Fig. 9. (A) Ta versus Nb concentration plot (log–log scale to show large variations). (B) Ho versus Y concentration plot. Data sources can be found in Appendix 2 (online).

are essential for assessing whether there is significant HFSE depletion using "spidergrams", which is a characteristic of island arc basalts. Figs. 5D and 9 show that with our own data Ta and Nb are highly correlated as expected. Literature data are of variable quality and there is no relation between data quality and year of publication. For example, the quality of data by Zhi and Feng (1992) is about the same as our data. However, Nb/Ta ratio of more recent data by Zhang et al. (2002) ranges from 15 to 128, and that of data by Fan et al. (2002) ranges from 10.7 to 15.1, deviating significantly from Nb/Ta ratio established by other analyses.

Fig. 9B shows Ho versus Y. Excellent correlation is evident. Our data again show excellent correlation between Ho and Y with Y/Ho ratio at 28.1 (±20%), similar to the BSE ratio of 28.9 (McDonough and Sun, 1995). Literature data show a total deviation of 40% in Y/Ho ratio, i.e., with less scatter than that on the Ta versus Nb diagram.

Because literature data (even very recent data) are of variable quality and it is difficult to evaluate the quality *a priori*, one cannot simply compile literature data to examine the enrichment or depletion of specific elements (such as Nb, Ta, Ba, and Rb). In the future it will be important for authors to acquire more trace element data and to follow the standard procedures (Goldstein et al., 2003) in presenting geochemical data. In discussion below, we will emphasize our own trace element data (although limited) to investigate source characteristics and address the origin of volcanic rocks in NE China.

4.3.2. Trace element characteristics from spidergrams

Trace element abundances normalized to BSE (McDonough and Sun, 1995) are plotted in spidergrams in Fig. 6. For all samples, there is no significant (meaning outside analytical uncertainty) Eu anomaly, and there is Th depletion to various degrees. Except for WDLC and EKS, there is no depletion of Nb and Ta. Although Zr and Hf are not included in the diagrams as outlined in section 3.2, examination of the data shows that there is no depletion. There is occasional depletion of Ba and K in some samples, which is opposite to enrichment of large ion lithophile elements in subduction-related basalts, but is largely consistent with other intraplate volcanics, such as East Australia basalts.

In summary, there is no depletion of high field strength elements (except for WDLC and EKS, which will be addressed later) and no enrichment of large ion lithophile elements in most basalts from Greater NE China. Hence, there is no geochemical evidence for the involvement of subduction slab in the production of Greater NE China basalts.

4.4. Variations among different volcanic fields

In this section, we use major and trace elements to further infer the partial melting conditions in the mantle and examine difference among volcanic fields. In order to infer mantle conditions, we correct for shallow level fractionation by adding olivine incrementally to a basalt until the Mg# of the basalt is 73%, roughly in equilibrium with mantle peridotite (e.g., Hart et al., 1997). The correction is not applied to basalt with MgO < 6 wt.%, nor to basalt that would require more than 30% additional olivine, because for such basalt olivine may not be the dominant mineral of low-pressure fractionation. Before correction, the ferric Fe content is assumed to be 10% of total Fe and major oxide total is normalized to 100%. $K_{D,Fe/Mg}$ and $K_{D,Mn/Mg}$ between olivine and melt are assumed to be 0.33 and 0.25 respectively (e.g.,

Roeder and Emslie, 1970; Jones, 1984). In plots discussed below, although plotting the corrected data changes the details, the overall trends are the same as plotting original data. That is, the correction does not significantly affect the diagrams and conclusions below, but makes it self-consistent to treat these melts as mantle-derived.

Compositional variations of mantle-derived basalts may be ascribed to (i) heterogeneity in the mantle, and/or (ii) the degree and (iii) depth of partial melting. (The depth affects the mineralogy such as presence of garnet.) Isotopic ratio variations are ascribed to mantle heterogeneity treated as a mixture of some end-members. Concentrations of major and trace elements of mantle-derived basalts (after correction of shallow depth fractionation) can be easily affected by the degree and depth of partial melting. Hence one often first investigates the effect of the degree and depth of partial melting of a homogeneous mantle (e.g., Shaw, 1970; Allegre et al., 1977; Zou and Zindler, 1996; Zou, 2000) even when there is isotopic heterogeneity (e.g., Hart et al., 1997), and only those features that cannot be explained by degree and depth of partial melting would be explained by mantle heterogeneity.

If the mantle source before melting is compositionally and mineralogically homogeneous, elements with different incompatibility would correlate. Plotting C_1/C_2 versus C_1 would result in a straight line (Allegre et al., 1977; Hofmann et al., 1986):

$$\frac{C_1}{C_2} = \left[D_2 - D_1\left(\frac{1-P_2}{1-P_1}\right)\right]\frac{C_1}{C_2^0} + \frac{C_1^0}{C_2^0}\left(\frac{1-P_2}{1-P_1}\right) \quad (1)$$

where C is concentration, D is the bulk partition coefficient of the minerals weighted in the proportions in the source, P is the bulk partition coefficient of the minerals weighted in the proportions in which they melt, subscripts 1 and 2 indicate elements 1 and 2, superscript 0 represents original value in the source.

Fig. 10A shows (La/Sm) ratio normalized to chondrite versus La concentration. For most volcanic fields (such as WDLC and EKS, MDJ and JX, JBH, LG, KD, and DT), La/Sm versus La is roughly a straight line. However, when all volcanic fields in Greater NE China are viewed together, recent Greater NE China basalts roughly follow a curved trend. East Australia basalts (Zhang et al., 2001) and Honolulu peralkaline basalts (Clague and Frey, 1982) also follow curved trends. East Australia basalts follow the similar trend as Greater NE China, but Honolulu basalts follow a different trend. The observations suggest that for a given volcanic field, the variation in the partition coefficients of La and Sm is small enough so that a linear trend is produced from a homogeneous source mantle. However, for the whole volcanic province (11 volcanic fields), the partition coefficients vary so that the overall trend is curved. The variation in the partition coefficients is attributed to the variation in mineralogy as well as mineral proportions in the source mantle (e.g., due to variation in the depth of melting). Other figures show similar relations, and the relation can be more curved if the difference in the degrees of incompatibility of the two elements is large. Furthermore, there can be more scatter if one of the elements shows anomalies in the spidergram.

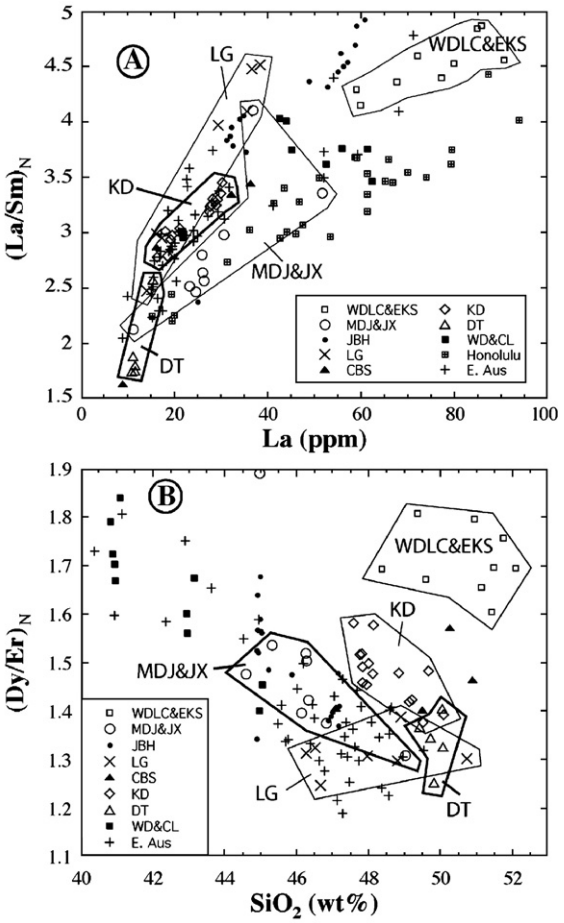

Fig. 10. (A) Normalized La/Sm ratio versus corrected La concentration. (B) Normalized (Dy/Er) ratio versus corrected SiO_2. Data are from this work.

The fractionation-corrected concentrations of incompatible elements such as Th and La, as well as trace element ratios such as La/Sm, increase with decreasing degree of partial melting. The SiO_2 activity of mantle partial melts decreases with increasing depth of partial melting (e.g. Carmichael et al., 1970; Carmichael, 2004)

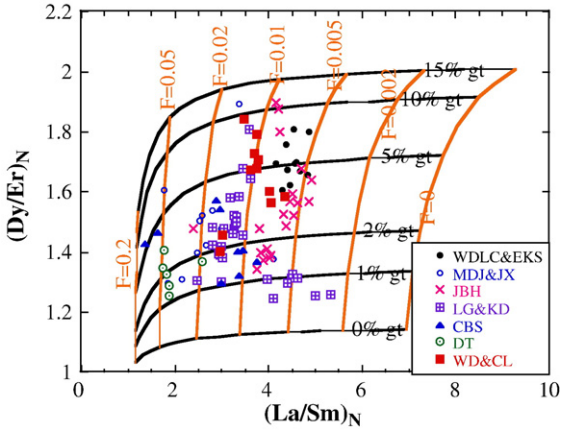

Fig. 11. Normalized (Dy/Er) ratio versus (La/Sm) ratio. The 2σ relative errors for La/Sm and (Dy/Er) ratio are 18% and 25% respectively. Data are from this work.

assuming olivine and orthopyroxene are coexisting in the mantle (very robust). Because calculation of SiO_2 activity requires knowledge of H_2O content in the melt (Carmichael, 2004) in equilibrium with the mantle, which is not available, we will simply use SiO_2 content to be a rough indicator of SiO_2 activity. Heavy rare earth elements may indicate the percentage of garnet in the mantle, which in turn is roughly correlated with depth of melting. Because Yb and Lu concentrations are not well analyzed in this work, we use Dy/Er ratio for this exercise.

In Fig. 11, normalized (Dy/Er) ratio is plotted against (La/Sm) ratio, together with calculated grids of the degree of partial melting and the percentage of garnet in the source region using forward modeling. This diagram is constructed by analogy to (Dy/Yb) versus (La/Sm) diagrams used by Fram and Lesher (1993). One difference is the use of proportion of garnet here instead of depth on constructing the grids because relating proportion of garnet with depth requires additional assumptions. The partition coefficients are from Donnelly et al. (2004). The diagram shows that the degree of partial melting ranges from 0.5% to 10% with lower degree of partial melting at WDLC, EKS, JBH, LG and KD, and higher degree of partial melting at MDJ, JX, DT and CBS (highest degree of melting). The high degree of partial melting at CBS suggests high temperature or high water content in the mantle, and is consistent with CBS being the largest volcano in Greater NE China. Because the variation in (Dy/Er) ratio is small, and 2σ error bar for (Dy/Er) ratio is about 25%, the proportion of garnet in the source region is not well resolved, but roughly in the range of 0 to 10%.

Fig. 10B shows normalized (Dy/Er) ratio versus corrected SiO_2. Both are related to the depth of mantle partial melting. A low SiO_2 means melting at greater depth. A high (Dy/Er) ratio means more garnet in the source and hence greater depth. Hence there should be a negative correlation between (Dy/Er) ratio and corrected SiO_2. This is indeed so in Fig. 10B, with subparallel and nearly identical trends for NE China and East Australia basalts, except for WDLC and EKS region.

Fig. 12 shows corrected La concentration and normalized La/Sm ratio versus corrected SiO_2 (roughly related to the depth of melting). There is negative correlation between La and SiO_2, and between La/Sm and SiO_2 for recent NE China basalts as well as East Australia basalts and Honolulu peralkaline basalts. (Again, WDLC and EKS are off the general trend.) The observed negative correlation can be explained by different degree of partial melting at different depth, with smaller degree at greater depth. Furthermore, at a given volcanic field, there is large variation in corrected La and SiO_2 content, as well as La/Sm ratio, indicating a large range of depth and degree of partial melting, and

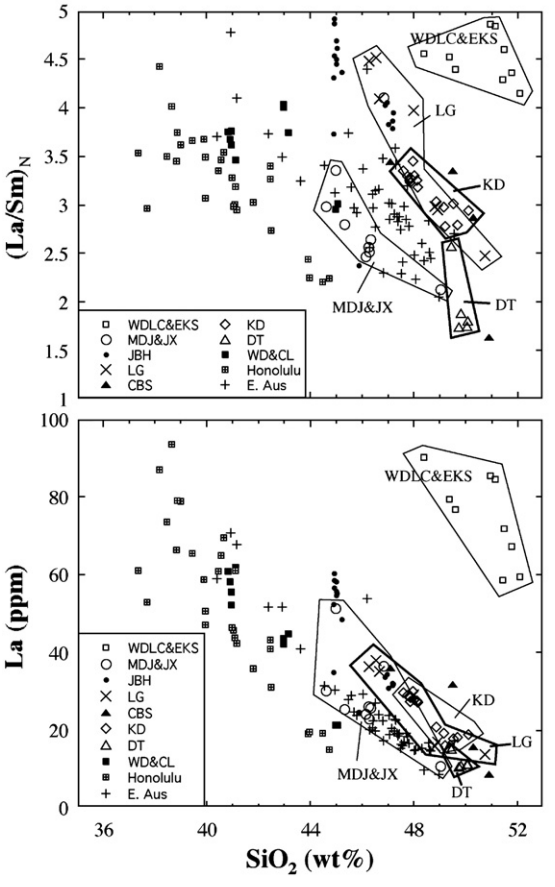

Fig. 12. Corrected La concentration and normalized (La/Sm) ratio versus corrected SiO_2. Data are from this work.

minimal mixing of melts generated at different depths. The different trends for various volcanic fields in Fig. 12 probably reflect different degrees of partial melting at a given depth (or a given SiO_2). That is, at a given depth (such as 70 km), the degree of partial melting is highest at WD, CL, MDJ, and JX, followed by DT, LG, CBS, KD, and JBH. WDLC and EKS are outliers, and have the highest SiO_2 content at the same (La/Sm) ratio or the same corrected La concentration. The results imply that there is regional difference in geothermal gradient or in volatile contents in the mantle, which led to the difference in the degrees of partial melting at the same depth.

4.5. WDLC and EKS

Basalts of WDLC and EKS are different in many aspects from the rest of recent basalts in Greater NE China. The differences are summarized below:

(i) Basalts of WDLC and EKS are potassic. Nevertheless, on trace element spidergram, there is no additional K enrichment. Hence the highly potassic nature is attributable to very small degree of partial melting.
(ii) La concentration and La/Sm ratios are high, suggesting very small degree of melting.
(iii) SiO_2 content in WDLC and EKS basalts is high relative to the incompatible trace element concentrations (Fig. 12), suggesting shallow depth of melting.
(iv) Depletion of Nb, Ta and Th suggests melting of continental lithosphere (Turner and Hawkesworth, 1995).
(v) Dy/Er ratio is high, suggesting garnet presence in the source region.
(vi) Isotopically, WDLC and EKS are near the extreme end of the LoMu isotopic end-member, similar to Smoky Buttes lamproites.

The above characteristics are best explained by small degrees of partial melting of the continental lithosphere at shallow depth in the presence of phlogopite and/or amphibole (Class and Goldstein, 1997). The inferred presence of garnet in the source region is difficult to reconcile with shallow depth, but might be due to garnet-bearing eclogite veins. If the mantle source region contains high water content, partial melting of the relatively cold lithosphere would be facilitated.

4.6. Depletion of large ion lithophile elements

Basalts from WD and CL show significant depletion (by about a factor of 2) of large ion lithophile elements (K and Ba). Furthermore, basalts from CBS display both depletion and enrichment of large ion lithophile elements. Because K and Ba are easily mobilized in fluid, the depletion (as well as occasional enrichment) may be attributed to fluid activity in the source mantle. Removal of fluid (dehydration) would deplete the large ion lithophile elements, and addition of fluid would enrich these elements. It is hence important in the future to investigate water content in the mantle source region or in pre-eruptive basalt.

4.7. Summary and synthesis

4.7.1. Plume/hotspot volcanism?

He isotopic data presented in this work suggest that there is no high-$^3He/^4He$ mantle plume involved in NE China volcanism. Furthermore, seismic tomographic images of Zhao et al. (2004) show that the seismic velocity anomalies beneath volcanic fields are shallow, without any deep roots that would be consistent with a deep-seated hotspot or mantle plume. Hence, the plume or hot spot hypothesis for recent NE China volcanism does not have strong support.

4.7.2. Back-arc volcanism?

Seismic tomography (Zhao et al., 2004) shows that the Pacific plate subducts from Japan trench and gradually flattens at a depth of 400 to 600 km (in the transition zone) in the NE China volcanic region. The horizontal slab underlies the volcanic fields in greater NE China, consistent with the suggestion that recent NE China basalts are related to back-arc extension (e.g. Basu et al., 1991; Liu et al., 2001; Ren et al., 2002). The linear volcanic belt along Changbaishan is roughly parallel to Japan Trench, also consistent with the suggestion. However, there is no slab signature in recent NE China basalts. Classical back-arc basalts show affinities with island arc basalts with LILE enrichment and HFSE depletion, and this signature diminishes as the distance of back-arc spreading center to the island or continental arc increases (Taylor and Martinez, 2003). Therefore, the complete absence of slab signature may be attributed to the great distance (>1000 km) between NE China volcanic fields and Japan Arc. Hence, the back-arc extension hypothesis cannot be ruled out by geochemistry. Because there is no evidence for the involvement of slab fluid, partial melting in the mantle of NE China is not helped by water from dehydrated Pacific slab even if the volcanism is due to back-arc extension. Whether the slab and the subduction process are causing a corner flow in the big mantle wedge (Chen, personal communication) cannot be evaluated from geochemistry currently.

4.7.3. Volcanism due to asthenosphere upwelling when cross the Gravity Gradient Line?

This hypothesis was advanced by Niu (2005). In Fig. 1, one can see a sharp topographic boundary between the low-lying East China and high-lying West China. The boundary is slightly to the east of Daxing'anling in its north segment, and to the east of Erdos in its south segment. The boundary was referred to as the Gravity Gradient Line by Niu (2005). Niu (2005) argues that because the lithosphere thickness changes rapidly across the boundary, from about 150 km west of the boundary to about 80 km east of the boundary, the volcanism in Greater NE China is due to decompression from 150 km depth to 80 km depth when asthenospheric flow crosses the boundary from west to east. Although this model can explain the few volcanic activities on the immediate east of the Gravity Gradient Line, it does not explain volcanic activities on the west of the Line, nor does it explain the volcanic activities about 700 km to the east of the boundary.

4.7.4. Volcanism due to delamination of continental lithosphere?

Based on the presence of diamondiferous kimberlitic rocks, thermobarometry of mantle xenoliths found in kimberlites, and other lines of argument, the lithosphere thickness of the North China Craton (which extends to Liaoning of NE China; see the long-dashed line in Fig. 1) was about 200 km during Paleozoic (e.g., Menzies et al., 1993; Griffin et al., 1998; Menzies and Xu, 1998). At present, the lithosphere ranges from about 60 km in the Bohai region (Liu, 1987; Ma et al., 2002) to about 120 km (Xu et al., 1998b; Ma et al., 2002). One suggestion was that the thinning of the lithosphere during the Mesozoic brought hot asthenosphere closer to the surface, leading to decompressional melting. The localized distribution of the volcanic fields on the borders of NE China Plain may be attributed to the pathways for magma to come to the surface.

Although our data cannot pin down the exact origin, the weight of various lines of evidence, including the absence of high $^{3}He/^{4}He$ ratios, the lack of HFSE depletion and LILE enrichment, the diffuse distribution of volcanic rocks, the strongly alkaline nature of the volcanic rocks, the enrichment of incompatible elements, and the involvement of both asthenospheric and lithospheric mantle in mantle partial melting, seems to be most easily reconciled by diffuse volcanism due to lithosphere thinning. Nevertheless, it is possible that subduction played a role in thinning the lithosphere. For example, the current pile-up of the subducted slab at 400–700 km depth will eventually avalanche into the lower mantle (Tackley et al., 1993). When this happens, mantle convection would be enhanced, which might lead to erosion or delamination of a thick lithosphere. Similar pile-up and avalanche could have happened in the past and led to lithosphere thinning of North China Craton. This speculation may be evaluated through geodynamic mantle convection models.

There is a difficulty (or paradox) to account for volcanism in Greater NE China by delamination because delamination occurred mostly in NCKC, but volcanism in this region is mostly north of NCKC. Whether and how delamination in North China–Korea Craton could affect NE China will require future studies.

4.8. Future research directions

Accurate and detailed mapping of the volcanic rocks is the first and critical step for all subsequent investigations. Detailed geochronological investigations of volcanic history of individual volcanic fields based on mapping will be necessary to reveal the spatial-time evolution of volcanic activities. Both mapping and dating should be intensified in the future.

To further understand partial melting that produced the volcanos in Greater NE China, it will be important to determine the pre-eruptive water content in various volcanic fields. From the pre-eruptive water content in basalts, it may be possible to estimate H_2O/K_2O ratio in the mantle source, and the role of H_2O in controlling the depth and degree of partial melting. The regions with anomalous trace element patterns may be related to water and hydrous minerals in the mantle. For example, high water content in the mantle source would be consistent with and help to explain partial melting at relatively low temperatures in the lithospheric mantle in WDLC and EKS. Loss of a fluid component from the mantle source could explain the depletion of large ion lithophile elements in WD and CL.

Our preliminary modeling indicates that some CBS basalts formed by high degree of mantle partial melting, which is consistent with CBS being the largest volcano in Greater NE China. More systematic sampling and comprehensive investigation of major and trace elements is necessary to check whether this is true for the basement building stage of Mount Changbai. Furthermore, whether the high degree of partial melting is related to high water content in the mantle, or whether it is due a hotter mantle may be resolved by thermobarometry and determination of water content in the mantle.

A broader spatial coverage of the volcanic fields for $^{3}He/^{4}He$ analyses is clearly needed to rule out any role for a high $^{3}He/^{4}He$ mantle plume in the volcanism of NE

China. Particular attention needs to be paid to sample collection and analyses aimed at minimizing the contribution of cosmogenic ^{3}He.

Because reliable trace element data are still scarce, it will be important in the future to obtain high-quality trace element data for all volcanic fields. Accurate mapping of crustal and lithospheric thickness might help to relate compositional characteristics to geophysical properties.

Acknowledgments

We thank Bolu Jin, Jianbo Shao and other colleagues at Shenyang Geological Academy, Ruishan Li, Yaoqi Zhou, Shiyong Yan, Zhicong Zhang, Qitao Lv, Baoshu Piao, and Xiaochen Han for assistance in fieldwork. Informal discussion with Yigang Xu, Xinhua Zhou, and Haibo Zou was very helpful. Constructive reviews by Xinhua Zhou and Haibo Zou are greatly appreciated. The editor Yaoling Niu helped in manuscript revision and instructed us to shorten the manuscript and reference list. We thank John Lupton for access to the helium isotope lab in Newport, OR, which is supported by the NOAA Vents Program. This work was supported by the US National Science Foundation (EAR 02-28752 and 05-37598 to YZ, and OCE 02-41909 to DG), a Sokol International Summer Research Fellowship to Yang Chen by the University of Michigan, and the Natural Science Foundation of China (NSFC grant 405118005).

Appendix A. Supplementary data

Supplementary data associated with this article can be found, in the online version, at doi:10.1016/j.lithos.2006.09.015.

References

Allegre, C.J., Treuil, M., Minster, J.F., Minster, B., Albarede, F., 1977. Systematic use of trace-element in igneous process.1. fractional crystallization processes in volcanic suites. Contributions to Mineralogy and Petrology 60, 57–75.

Basu, A.R., Wang, J.W., Huang, W.K., Xie, G.H., Tatsumoto, M., 1991. Major element, REE, and Pb, Nd and Sr isotopic geochemistry of Cenozoic volcanic rocks of eastern China: implications for their origin from suboceanic-type mantle reservoirs. Earth and Planetary Science Letters 105, 149–169.

Carmichael, I.S.E., 2004. The activity of silica, water, and the equilibration of intermediate and silicic magmas. American Mineralogist 89, 1438–1446.

Carmichael, I.S.E., Nicholls, J., Smith, A.L., 1970. Silica activity in igneous rocks. American Mineralogist 55, 246–263.

Choi, S.H., Kwon, S.-T., Mukasa, S.B., Sagong, H., 2005. Sr–Nd–Pb isotope and trace element systematics of mantle xenoliths from Late Cenozoic alkaline lavas, South Korea. Chemical Geology 221, 40–64.

Clague, D., Frey, F.A., 1982. Petrology and trace element geochemistry of the Honolulu volcanics, Oahu: Implications for the oceanic mantle below Hawaii. Journal of Petrology 23, 447–504.

Clarke, W.B., Beg, M.A., Craig, H., 1969. Excess ^{3}He in the sea: evidence for terrestrial primordial helium. Earth and Planetary Science Letters 6, 213–220.

Class, C., Goldstein, S.L., 1997. Plume-lithosphere interactions in the ocean basins: constraints from the source mineralogy. Earth and Planetary Science Letters 150, 245–260.

Class, C., Goldstein, S.L., 2005. Evolution of helium isotopes in the Earth's mantle. Nature 436, 1107–1112.

Deng, J.F., Zhao, H.L., Mo, X.X., Wu, Z.S., Luo, Z.H., 1996. Continental Roos-Plume Tectoncis: A Key to Continental Dynamics. Geology Press, p. 110 (in Chinese).

Deng, J.F., Mo, X.X., Zhao, H.L., Wu, Z.X., Luo, Z.H., Su, S.G., 2004. A new model for the dynamic evolution of Chinese lithosphere: 'continental roots-plume tectonics'. Earth-Science Reviews 65, 223–275.

Doe, B.R., Leeman, W.P., Christiansen, R.L., 1982. Lead and strontium isotopes and related trace-elements as genetic tracers in the upper Cenozoic rhyolite–basalt association of the Yellowstone Plateau volcanic field. Journal of Geophysical Research B87, 4785–4806.

Donnelly, K.E., Goldstein, S.L., Langmuir, C.H., Spiegelman, M., 2004. Origin of enriched ocean ridge basalts and implications for mantle dynamics. Earth and Planetary Science Letters 226, 347–366.

Douglass, J., Schilling, J.G., 2000. Systematics of three-component, pseudo-binary mixing lines in 2D isotope ratio space representations and implications for mantle plume–ridge interaction. Chemical Geology 163, 1–23.

Fan, Q.C., Hooper, P.R., 1989. The mineral chemistry of ultramafic xenoliths of Eastern China: implications for upper mantle composition and the Paleogeotherms. Journal of Petrology 30, 1117–1158.

Fan, Q.C., Sui, J.L., Liu, R.X., Wei, H.Q., Li, D.M., Sun, Q., Li, N., 2002. Periods of Quarternary volcanic activity in Longgang area, Jilin province. Acta Petrologica Sinica 18, 495–500 (in Chinese).

Fram, M.S., Lesher, C.E., 1993. Geochemical constraints on mantle melting during creation of the North Atlantic basin. Nature 363, 712–715.

Goldstein, S.L., Deines, P., Oelkers, E.H., Rudnick, R.L., Walter, L.M., 2003. Standards for publication of isotope ratio and chemical data in Chemical Geology. Chemical Geology 202, 1–4.

Graham, D.W., 2002. Noble gas isotope geochemistry of mid-ocean ridge and ocean island basalts: characterization of mantle source reservoirs. Reviews in Mineralogy and Geochemistry 47, 247–317.

Graham, D.W., Larsen, L.M., Hanan, B.B., Storey, M., Pedersen, A.K., Lupton, J.E., 1998. Helium isotope composition of the early Iceland mantle plume inferred from the Tertiary picrites of West Greenland. Earth and Planetary Science Letters 160, 241–255.

Griffin, W.L., Zhang, A., O'Reilly, S.Y., Ryan, C.G., 1998. Phanerozoic evolution of the lithosphere beneath the Sino-Korean Craton. In: Flower, M.F.J., Chung, S.L., Lo, C.H., Lee, T.Y. (Eds.), Mantle Dynamics and Plate Interactions in East Asia. American Geophysical Union, p. 27.

Hannah, R.S., Vogel, T.A., Patino, L.C., Alvarado, G.E., Perez, W., Smith, D.R., 2002. Origin of silicic volcanic rocks in Central Costa Rica: a study of a chemically variable ash-flow sheet in the Tiribi Tuff. Bulletin of Volcanology 64, 117–133.

Hart, S.R., 1992. Mantle plumes and entrainment: isotopic evidence. Science 256, 517–520.
Hart, S.R., Blusztajn, J., LeMasurier, W.E., Rex, D.C., 1997. Hobbs Coast Cenozoic volcanism: implications for the West Antarctic rift system. Chemical Geology 139, 223–248.
Hauri, E.H., Whitehead, J.A., Hart, S.R., 1994. Fluid dynamic and geochemical aspects of entrainment in mantle plumes. Journal of Geophysical Research B99, 24275–24300.
Hawkesworth, C.J., Kempton, P.D., Rogers, N.W., Ellam, R.M., van Calsteren, P.W., 1990. Continental mantle lithosphere, and shallow level enrichment processes in the Earth's mantle. Earth and Planetary Science Letters 96, 256–268.
Hilton, D.L., Craig, H., 1989. A helium isotope transect along the Indonesian archipelago. Nature 342, 906–908.
Hilton, D.R., Gronvold, K., Macpherson, C.G., Castillo, P.R., 1999. Extreme $^{3}He/^{4}He$ ratios in northwest Iceland: constraining the common component in mantle plumes. Earth and Planetary Science Letters 173, 53–60.
Hofmann, A.W., Jochum, K.P., Seufert, M., White, W.M., 1986. Nb and Pb in oceanic basalts: new constraints on mantle evolution. Earth and Planetary Science Letters 79, 33–45.
Jin, B.L., Zhang, X.Y., 1994. Researching Volcanic Geology in Mount Changbai. Dongbei Chaoxianminzu Jiaoyu Press.
Jones, J.H., 1984. Temperature- and pressure-independent correlations of olivine/liquid partition coefficients and their application to trace element partitioning. Contributions to Mineralogy and Petrology 88, 126–132.
Knaack, C., Cornelius, S.B., Hooper, P.R., 1994. Trace element analyses of rocks and minerals by ICP-MS. Lab Technical Notes. GeoAnalytical Lab, Washington State University. http://www.wsu.edu/~geology/geolab/note/icpms.html.
Kurz, M.D., 1986. In situ production of terrestrial cosmogenic helium and some applications to geochronology. Geochimica et Cosmochimica Acta 50, 2855–2862.
Kurz, M.D., Jenkins, W.J., Hart, S.R., 1982. Helium isotopic systematics of oceanic islands and mantle heterogeneity. Nature 297, 43–46.
Kurz, M.D., Jenkins, W.J., Hart, S.R., Clague, D., 1983. Helium isotopic variations in volcanic rocks from Loihi Seamount and the island of Hawaii. Earth and Planetary Science Letters 66, 388–406.
Lai, Y., Liu, Y.L., Huang, B.L., Chen, Y.J., 2005. The characteristics of noble gases in mantle-derived xenoliths in Wudalianchi and Kuandian, NE China: MORB-like mantle and metasomatized mantle. Acta Petrologica Sinica 21, 1373–1381 (in Chinese).
Le Bas, M.J., Le Maitre, R.W., Streckeisen, A., Zanettin, B., 1986. A chemical classification of volcanic rocks based on the Total Alkali-Silica diagram. Journal of Petrology 27, 745–750.
Li, Y.H., Li, J.C., Song, H.B., Guo, L.H., 2002. Helium isotope studies of the mantle xenoliths and megacrysts from the Cenozoic basalt in the eastern China. Science in China 45, 174–183.
Liu, G.D., 1987. The Cenozoic rift system of the North China Plain and the deep internal process. Tectonophysics 133, 277–285.
Liu, R.X. (Ed.), 1992. Geochoronlogy and Geochemistry of Cenozoic Volcanic Rocks in China. Seismology Press, Beijing (in Chinese).
Liu, R.X. (Ed.), 1995. Volcanic Activities and Human Environment. Seismology Press, Beijing.
Liu, J.Q., 1999. Chinese Volcanos. Science Press, Beijing. (in Chinese).
Liu, B.L., Chen, Y.W., Zhu, B.Q., 1989. Petrogenesis and mantle geochemical features of Cenozoic basalts in Jinpohu area, NE China: evidences from Sr-Nd-Pb isotopes and trace elements. Geochemistry 20 (1), 8–19 (in Chinese).
Liu, J.Q., Han, J.T., Fyfe, W.S., 2001. Cenozoic episodic volcanism and continental rifting in northeast China and possible link to Japan Sea development as revealed from K–Ar geochronology. Tectonophysics 339, 385–401.
Ma, L.F., Qiao, X.F., Min, L.R., Fan, B.X., Ding, X.Z. (Eds.), 2002. Geology Maps of China. Geology Press, Beijing. 348 pp.
Mahoney, J.J., White, W.M., Upton, B.G.J., Neal, C.R., Scrutton, R.A., 1996. Beyond EM-1: lavas from Afanasy–Nikitin Rise and the Crozet Archipelago, Indian Ocean. Geology 24, 615–618.
McDonough, W.F., Sun, S.S., 1995. The composition of the Earth. Chemical Geology 120, 223–253.
Menzies, M.A., Xu, Y.G., 1998. Geodynamics of the North China Craton. In: Flower, M.F.J., Chung, S.L., Lo, C.H., Lee, T.Y. (Eds.), Mantle Dynamics and Plate Interactions in East Asia. Geodynamics Series. American Geophysical Union, Washington, D.C., pp. 155–165.
Menzies, M.A., Fan, W., Zhang, M., 1993. Paleozoic and Cenozoic lithoprobes and the loss of >120 km of Archean lithosphere, Sino-Korean craton, China. In: Prichard, H.M., Alabaster, T., Harris, N.B.W., Neary, C.R. (Eds.), Magmatic Processes and Plate Tectonics. Geological Society Special Publications, pp. 71–81.
Niu, Y.L., 2005. Generation and evolution of basaltic magmas: some basic concepts and a new view on the origin of Mesozoic–Cenozoic basaltic volcanism in Eastern China. Geological Journal of China Universities 11, 9–46.
O'Brien, H.E., Irving, A.J., McCallum, I.S., Thirlwall, M.F., 1995. Strontium, neodymium, and lead isotopic evidence for the interaction of post-subduction asthenospheric potassic mafic magmas of the Highwood Mountains, Montana, USA, with ancient Wyoming craton lithospheric mantle. Geochimica et Cosmochimica Acta 59, 4539–4556.
Peng, Z.C., Zartman, R.E., Futa, K., Chen, D.G., 1986. Pb-, Sr- and Nd-isotopic systematics and chemical characteristics of Cenozoic basalts, Eastern China. Chemical Geology 59, 3–33.
Porcelli, D.R., Stone, J.O.H., O'Nions, R.K., 1987. Enhanced $^{3}He/^{4}He$ ratios and cosmogenic helium in ultramafic xenoliths. Chemical Geology 64, 25–33.
Porcelli, D.R., O'Nions, R.K., Galer, S.J.G., Cohen, A.S., Mattey, D.P., 1992. Isotopic relationships of volatile and lithophile trace elements in continental ultramafic xenoliths. Contributions to Mineralogy and Petrology 110, 528–538.
Poreda, R., Craig, H., 1989. Helium isotope ratios in circum-Pacific volcanic arcs. Nature 338, 473–478.
Ren, J.Y., Tamaki, K., Li, S., Zhang, J.X., 2002. Late Mesozoic and Cenozoic rifting and its dynamic setting in Eastern China and adjacent areas. Tectonophysics 344, 175–205.
Roeder, P.L., Emslie, R.F., 1970. Olivine-liquid equilibrium. Contributions to Mineralogy and Petrology 29, 275–289.
Sengor, A.M.C., Natal'in, B.A., 1996. Paleotectonics of Asia: fragments of a synthesis. In: Yin, A., Harrison, T.M. (Eds.), The Tectonic Evolution of Asian. Cambridge University Press, New York, pp. 486–640.
Shangguan, Z.G., Du, J.K., Zang, W., 1998. Modern hot spring geochemistry at the Tanlu fault and Jiaoliao block in eastern China. Science in China Series. D 41, 87–94.
Shaw, D.M., 1970. Trace element fractionation during anatexis. Geochimica et Cosmochimica Acta 34, 237–243.
Stracke, A., Hofmann, A.W., Hart, S.R., 2005. FOZO, HIMU, and the rest of the mantle zoo. Geochemistry, Geophysics, Geosystems 6 (5). doi:10.1029/2004GC000824.
Tackley, P.J., Stevenson, D.J., Glatzmaier, G.A., Schubert, G., 1993. Effects of an endothermic phase transition at 670 km depth in a

spherical model of convection in the Earth's mantle. Nature 361, 699–704.

Taylor, B., Martinez, F., 2003. Back-arc basin basalt systematics. Earth and Planetary Science Letters 210, 481–497.

Tu, K., Xie, G.H., Zhang, M., Wang, J.W., Flower, M.F.J., Carlson, R.W., 1992. Sr, Nd and Pb isotopic compositions of Cenozoic basalt in East China. In: Liu, R.X. (Ed.), Cenozoic Basalt in China: Geochronology and Geochemistry. Seismology Press, Beijing, pp. 330–338 (in Chinese).

Turner, S., Hawkesworth, C., 1995. The nature of the sub-continental mantle: constraints from the major-element composition of continental flood basalts. Chemical Geology 120, 295–314.

Wilde, S.A., Zhou, X.H., Nemchin, A.A., Sun, M., 2003. Mesozoic crust–mantle interaction beneath the North China craton: a consequence of the dispersal of Gondwanaland and accretion of Asia. Geology 31, 817–820.

Wu, M.B., Wang, X.B., Ye, X.R., Zhang, M.J., 2003. Noble gas isotopic compositions of Cenozoic volcanics and mantle-derived xenoliths from Kuandian in Liaoning Province and their significance. Acta Petrologica et Mineralogica 22, 254–258 (in Chinese).

Xu, S., Liu, C.Q., 2002. Noble gas abundances and isotopic compositions in mantle-derived xenoliths, NE China. Chinese Science Bulletin 47, 755–760.

Xu, S., Nagao, K., Uto, K., Wakita, H., Nakai, S., Liu, C.Q., 1998a. He, Sr and Nd isotopes of mantle-derived xenoliths in volcanic rocks of NE China. Journal of Asian Earth Sciences 16, 547–556.

Xu, Y.G., Menzies, M.A., Vroon, P., Mercier, J.C., Lin, C., 1998b. Texture–temperature–geochemistry relationship in the upper mantle as revealed from spinel peridotite xenoliths from Wangqing, N.E. China. Journal of Petrology 39, 469–493.

Yin, A., Harrison, M. (Eds.), 1996. The Tectonic Evolution of Asia. Cambridge University Press, Cambridge, England. 666 pp.

Yokochi, R., Marty, B., Pik, R., 2005. High $^{3}He/^{4}He$ ratios in peridotite xenoliths from SW Japan revisited: evidence for cosmogenic ^{3}He released by vacuum crushing. Geochemistry, Geophysics, Geosystems 6 (1). doi:10.1029/2004GC000836.

Zhang, M., Menzies, M.A., Suddaby, P., Thirlwall, M.F., 1991. EM1 signature from within the post-Archaean subcontinental lithospheric mantle: Isotopic evidence from the potassic volcanic rocks in NE China. Geochemical Journal 25, 387–398.

Zhang, M., Stepehson, P.J., O'Reilly, S.Y., McCulloch, M.T., Norman, M., 2001. Petrogenesis and geodynamic implications of late Cenozoic basalt in North Queensland, Australia: trace-element and Sr–Nd–Pb isotope evidence. Journal of Petrology 42, 685–719.

Zhang, Z., Feng, C., Li, Z., Li, S., Xin, Y., Li, Z., Wang, X., 2002. Petrochemical study of the Jingpohu Holocene alkali basaltic rocks, northeastern China. Geochemical Journal 36, 133–153.

Zhao, D.P., Lei, J.S., Tang, R.Y., 2004. Origin of the Changbai intraplate volcanism in Northeast China: Evidence from seismic tomography. Chinese Science Bulletin 49, 1401–1408.

Zhi, X.C., Feng, J.L., 1992. Geochemistry of Hannuoba basalt. In: Liu, R.-X. (Ed.), Geochoronlogy and Geochemistry of Cenozoic Volcanic Rocks in China. Dizhen Chubanshe, Beijing, pp. 114–148 (in Chinese).

Zou, H.B., 2000. Modeling of trace element fractionation during non-modal dynamic melting with linear variations in mineral/melt distribution coefficients. Geochimica et Cosmochimica Acta 64, 1095–1102.

Zhou, X.H., Armstrong, R.L., 1982. Cenozoic volcanic rocks of eastern China— secular and geographic trends in chemistry and strontium isotopic composition. Earth and Planetary Science Letters 58, 301–329.

Zhou, X.H., Zhu, B.Q., 1992. Cenozoic basalts in eastern China: isotopic systematics and mantle geochemical zoning. In: Liu, R.X. (Ed.), Geochronology and Geochemistry of Cenozoic Volcanic Rocks in Eastern China. Seismological Press, Beijing, pp. 366–391 (in Chinese).

Zou, H.B., Zindler, A., 1996. Constraints on the degree of dynamic partial melting and source composition using concentration ratios in magmas. Geochimica et Cosmochimica Acta 60, 711–717.

Zou, H., Zindler, A., Xu, X., Qi, Q., 2000. Major, trace element, and Nd, Sr and Pb isotope studies of Cenozoic basalts in SE China: mantle sources, regional variations, and tectonic significance. Chemical Geology 171, 33–47.